Unconventional optical Tamm states in metal-terminated three-dimensional photonic crystals

Alexander V. Korovin[1,2] and Sergei G. Romanov[3,4,*]

[1]*Laboratoire Génie Électrique et Électronique de Paris, 11 rue Joliot Curie, Plateau de Moulon, 91192 Gif sur Yvette, France*
[2]*Institute for Physics of Semiconductors, National Academy of Sciences of Ukraine, 45 Nauki Prospect, Kiev 03028, Ukraine*
[3]*Ioffe Physical Technical Institute, 194021, Polithekhnicheskaya ul., 26, St. Petersburg, Russia*
[4]*Institute of Particle Technology, University of Erlangen-Nuremberg, Haberstrasse 9a, 91058 Erlangen, Germany*

(Received 30 November 2015; revised manuscript received 15 February 2016; published 29 March 2016)

Unconventional optical Tamm surface states have been demonstrated in transmission and reflectance spectra of three-dimensional opal photonic crystals coated by thin metal films. These states appear in registry with diffraction resonances and localize the electromagnetic energy in asymmetric resonators formed by stacks of lattice planes and metal semishells. Tamm defect states provide the bypass for light at the edges of the Bragg diffraction resonances and thus reduce the diffraction efficiency. Despite the hidden nature of this effect, its magnitude is comparable to the extraordinary transmission associated with the surface-plasmon polaritons that are simultaneously excited at the surfaces of the corrugated metal films.

DOI: 10.1103/PhysRevB.93.115440

I. INTRODUCTION

Photonic crystals are the optical materials with a periodical pattern of a dielectric constant on a wavelength scale. They are capable of controlling the strength of light-matter interaction and molding the light flow. The photonic band structure is the principal phenomenon that determines the functionality of such crystals. It emerges in photonic crystals in a similar manner to electron energy bands of solids. Photonic bands are composed of eigenfunctions or Bloch modes, the complex field structure of which allows them to propagate in the crystal without scattering. Conveniently, changing the material pattern, such as the dielectric contrast, symmetry, and dimensionality [1] is used to modify the optical properties of photonic crystals.

In perfectly crystallized but finite atomic lattices, Bloch modes suffer scattering at the crystal surface due to the lack of the translation invariance of electron wave functions. Since the crystal surface operates as a lattice defect one can expect the respective defect energy state in the forbidden zone [2]. Such states, called Tamm defect states, compromise the operation of electronic devices, especially the ones which contain multiple interfaces, such as superlattices [3], by providing the bypass for the current flow. Expectedly, photonic crystals meet similar complications with the lattice interruption.

The technological advantage of photonic crystals is the possibility for more precise controlling of their surfaces compared to that in atomic crystals in proportion to the operating wavelength. This circumstance facilitates attaining the desired functionality of photonic crystals by manipulations with surface electromagnetic excitations and, in particular, by exploiting surface defects. The surface engineering approach enables the heterogeneous crystals with functional interfaces [4,5].

Electromagnetic surface waves are localized at both sides of the interface between materials with negative and positive permittivities and/or permeabilities, e.g., metals and dielectrics [6]. Being evanescent waves, they do not participate in the energy transport in either of the interfacing media. In metals, the wave propagation is suppressed due to the dominating imaginary wave number, whereas in dielectrics the wave propagation is prohibited if the tangential component of the wave vector falls outside the radiative zone. Coupling of evanescent waves to transient light requires special devices, e.g., prisms or gratings [7].

Photonic crystals enrich the toolbox for designing and exploiting surface waves. On one hand, the coupling device, namely, the periodic lattice, is the integral part of two- and three-dimensional photonic crystals. The respective evanescent waves at the surfaces of multidimensional photonic crystals have been theoretically predicted and experimentally observed [8–12]. The relative isolation of such waves from the modes in free space is used to realize, e.g., high quality factor surface resonators [13]. On the other hand, at photonic band-gap frequencies photonic crystals operate as mirrors, which reject the light penetration in the volume, i.e., they functionally replace metals. Moreover, they can play the role of materials with either negative permittivity or negative permeability [14].

In the first approximation, photonic crystals are considered as Bragg multilayers. In order to localize light in the space one can join the Bragg and the metal mirrors [15,16]. Such an asymmetric resonator confines light in the spectral range of the photonic stop band. The functionality of the respective resonance is similar to the properties of the defect optical state in the photonic band gap [17]. In particular, this state reveals itself as the band of high transmission in the transmission dip of the photonic stop band and as the band of low reflection in the respective reflection maximum. This defect state is called the optical Tamm state or the Tamm plasmon polariton [17]. Contrary to many other surface electromagnetic excitations, the Tamm plasmon polariton does not require phase matching with the wave vector of incident light and manifests itself for both transverse electric and transverse magnetic polarizations.

The current consensus is that the idea of optical Tamm states is exhaustively realized in one-dimensional photonic crystals (Bragg mirrors), which are terminated either by a metal mirror or by another Bragg mirror with the overlapping stop band [8,16]. Applications of Tamm states are

*sergey.romanov@fau.de

in line with those of conventional Fabry-Pérot resonators, e.g., polariton lasers [18] or perfect absorbers [19]. The advantages of surface-state engineering are the following: (i) the structure of a photonic crystal remains undisturbed, but (ii) the possibility of further modification, e.g., by impregnation interstitials with guest materials, is preserved, and (iii) the metal coating itself can be tuned independently and remains available for postdeposition modification, e.g., by patterning.

Is there any reason to try three-dimensional photonic crystals? *A priori*, the answer is not clear because of the interplay of many factors. First, one can expect a weaker effect because crystal planes are not continuous compared to homogeneous layers of the Bragg mirror, moreover, the three-dimensional patterning is prone to fabrication-related irregularities leading to incoherent scattering. Second, three-dimensional crystals possess much richer composition of Bloch modes compared to one-dimensional ones. All of them will suffer surface scattering, but, evidently, the conditions for Tamm state formation are not satisfied for noncoplanar metal and Bragg mirrors. Third, patterning of three-dimensional crystals offers grating coupling to evanescent surface modes. Nevertheless, only the discrete set of surface modes can be supported in agreement with the lattice symmetry. Fourth, the related corrugation is provocative for the excitation of surface modes at the metal-photonic crystal interface, e.g., surface-plasmon polaritons, which can potentially interact with other modes of the architecture.

To investigate optical Tamm states in metal-terminated three-dimensional photonic crystals we used opal crystals, which are the face-centered-cubic (fcc) lattices of closely packed dielectric spheres [20]. The opal lattice can be decomposed on particular Bragg mirrors so that each set of crystal planes operates in the same way as a Bragg multilayer mirror and provides a diffraction resonance [21]. In particular, thin-film opals can be described as a set of (111) crystal planes facing the film surface, hence, they are parallel to a metal mirror. If the mirror is flat, as it occurs when an opal is crystallized on a metal film-coated flat substrate, properties of the respective asymmetric resonator can be referred back to conventionally studied metal-coated Bragg mirrors. Oppositely, if the metal film is deposited on the opal surface, the metal adopts the periodical corrugation and forms a hexagonal lattice of dielectric core-metal semishells. Such a lattice of interconnected semishells can be considered itself as the planar two-dimensional plasmon-polaritonic crystal [22,23]. Taken together plasmonic and photonic crystals form a hybrid crystal, optical spectra of which contain both interface and diffraction resonances in contrast to merely diffraction resonances in spectra of all-dielectric photonic crystals [24].

There are several reasons for the dissimilarity between the optical properties of the opal assembled on the planar metal film and the same opal coated with the metal film. First, in the former configuration the refractive index of the opal spheres vanishes at contact points with a metal film [25] in contrast to the continuous dielectric-metal contact in coated spheres of the latter configuration. This difference reverses the phase, which is accumulated by a wave along the round trip in the photonic crystal [26,27]. Second, if the corrugation of a metal film is comparable to the wavelength, the incident light is rather scattered by semishells in contrast to the specular reflection of a flat mirror [28]. Third, the efficiency of light coupling to surface-plasmon polaritons at the metal-opal interface is weak in the case of the proximity of a metal film to a dielectric grating but is strong in the case of a deeply profiled metal grating.

In this paper, we present the evidence of resonances, which appear in registry with diffraction resonances in transmission and reflectance spectra of metal-coated opals, and elaborate on the model explaining these resonances in terms of the Tamm states. Assuming that semishells provide the broad angle diagram of the backscattered light, we suggest that this process supports Tamm surface states associated with diffraction orders that approach the photonic crystal surface at oblique angles. These states we term as unconventional Tamm surface states.

II. EXPERIMENTAL TECHNIQUE

Studied opal films have been crystallized from 5% polydisperse poly(methyl methacrylate) (PMMA) spheres with diameters of 430 and 560 nm in the moving meniscus on hydrophilic glass substrates with the help of the acoustic noise agitation on microscope glass slides [29,30]. No sintering has been applied to avoid the lattice distortion. In order to prepare metal-terminated opals, 50-nm Au films or 30-nm Ag films were sputtered on top of opal films [31]. These samples are abbreviated as Au- and Ag-opals. Structurally, metal-coated opals retain the appearance of bare opal films [Fig. 1(a)], whereas the metal films on the spheres become evident at a higher magnification of the scanning electron microscope image [Fig. 1(b)]. Since the metal coating adopts the topology of the opal surface [Figs. 1(a) and 1(b)], it can be described as a planar lattice of metal semishells, which are interconnected with each other by six metal bridges.

Optical spectra of hybrids have been obtained under the illumination by the collimated ∼1-mm-diameter beam of white light from a tungsten halogen lamp. Angle-resolved transmission spectra were acquired by the fixed grating spectrometers at different angles of light incidence θ in the range from $-80°$ to $80°$ with respect to the film normal with a step of $0.5°$. Linear polarizers and analyzers have been used to separate s or p polarizations with the electrical field oriented, respectively, either perpendicular or parallel to the plane of light incidence. Reflectance spectra have been measured through the glass substrate, and no corrections of the reflectance magnitude to the reflectance at the glass-air interface have been applied. The thicknesses of the opal films were determined by counting the number of Fabry-Pérot oscillations between (111) and its second-order (222) resonances. Diffraction resonances have been labeled according to the Miller indices of the corresponding fcc lattice planes.

For the sake of comparison, all spectra are plotted as a function of the reduced frequency in dimensionless units D/λ, where D is the diameter of the opal spheres. The plane of light incidence has been azimuthally oriented with respect to the lattice of the opal using the surface diffraction pattern to perform measurements in the ΓWLW cross section of the Brillouin zone [Fig. 1(c)]. The symmetry of spectra obtained

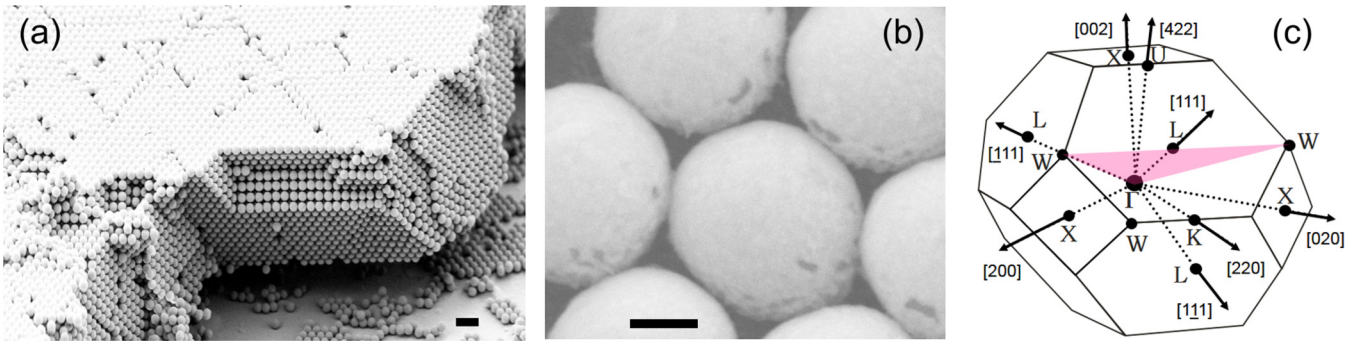

FIG. 1. Structure of hybrid photonic crystals. (a) Scanning electron microscope (SEM) image of an opal film (430-nm PMMA beads) top coated with a 50-nm Ag film. Scale bar—1000 nm. (b) SEM image of 30-nm-thick Ag semishells on 625-nm spheres. Metal bridges are resolved. Scale bar—200 nm. (c) Brillouin zone of the fcc lattice with labels at high-symmetry points. The corresponding directions in the real-space lattice are marked with arrows and Miller indices of respective lattice vectors. The shaded region corresponds to the scanning plane of the incidence in the reciprocal space.

within this cross section with respect to reversing the angle of light incidence has been used to align bare and metal-coated opal films. The precise alignment of the incidence plane is the necessary condition for the correct visualization of defect states by calculating the change in the light attenuation at a diffraction minimum after administering a metal coating. Dispersions of diffraction resonances in the opal lattice have been fitted using the Bragg-Snell law and assuming the (111) interplane distance in the fcc lattice as $d_{111} = 0.816D$.

To model the Tamm state in complex three-dimensional structures we reduced the opal film to the one-dimensional (111) multilayer. The transfer-matrix method has been used to derive the necessary conditions for the observation of the Tamm state in the stop-band interval of transmission/reflectance spectra of the Bragg mirror possessing the averaged dielectric permittivity profile along the [111] axis of the opal crystal. Then, in order to illustrate the role of the metal film corrugation, we calculated the field distribution and light-scattering diagrams of semishells in the framework of the finite-difference time-domain method [32] using the LUMERICAL software [33]. The optical constants of gold were adopted from the literature [34].

III. TRANSMISSION AND REFLECTANCE SPECTRA OF METAL-TERMINATED OPAL FILMS

Most of the resonances observed in optical spectra of a metal-terminated opal are the diffraction resonances at different lattice planes [35]. The immediate effect of gold coating is the strong reduction of light transmission in a Au opal compared to that of a bare opal film. Nevertheless, the diffraction resonances of the opal photonic crystals remain visible. In Figs. 2(a) and 2(b), which represent the transmission maps of a Au-opal hybrid assembled from 560-nm spheres and coated with a 50-nm gold layer, these resonances are approximated by lines calculated using the Bragg-Snell law for the diffraction in the fcc lattice of touching spheres,

$$\lambda_{hkl} = 2d_{hkl}n_{\text{eff}}\sqrt{1-\sin^2 r_{hkl}}, \qquad (1)$$

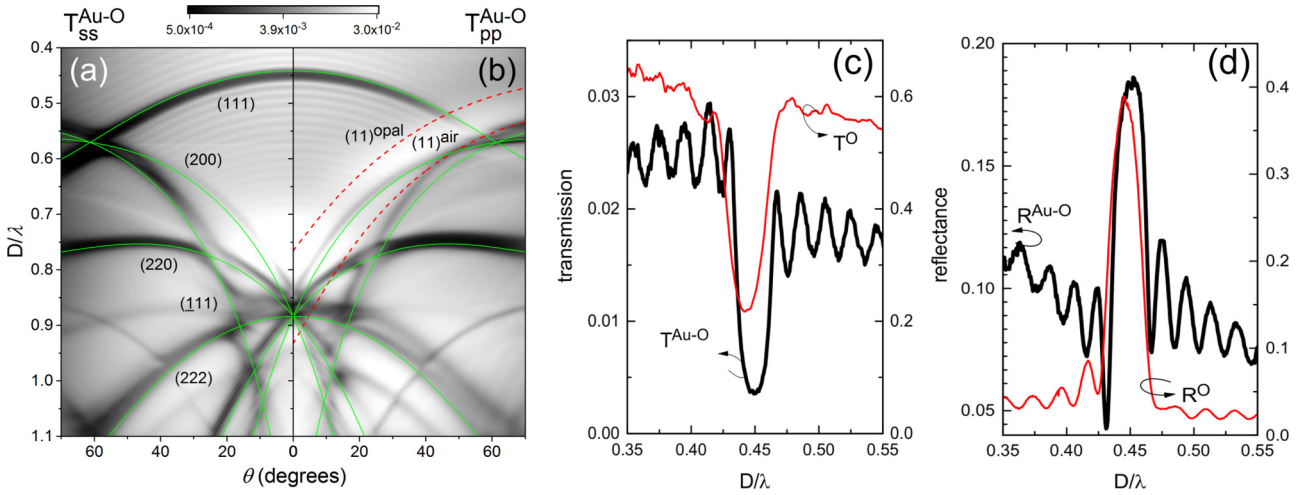

FIG. 2. Surface modes in the optical spectra. (a) and (b) Transmission maps of 50-m Au opals (560-nm spheres) in s- and p-polarized light, respectively. The solid lines labeled with Miller indices are the dispersions of Bragg resonances of the fcc lattice of spheres. The dotted lines mark the dispersions of (11) branches of surface-plasmon polaritons at the air and opal interfaces of the Au film. (c) and (d) Transmission and reflectance spectra of 50-nm Au-coated (thick line) and bare (thin line) opals assembled from 560-nm spheres obtained at the normal light incidence in the spectral range of the (111) diffraction resonance.

where $d_{hkl} = \sqrt{2}D/\sqrt{(h^2+k^2+l^2)}$ is the interplane distance for the (hkl) planes and the internal angle of incidence r_{hkl} relates to the external angle via Snells' law $n_{\text{eff}} \sin(r_{111}) = n_{\text{air}} \sin(\theta)$. The low-frequency (111) resonance, which produces the minimum at $D/\lambda \approx 0.46$ for the normal light incidence of $\theta = 0^\circ$ to the opal surface, is the diffraction resonance of the (111) Bragg multilayer [curve T^{O} in Fig. 2(c)].

The metal coating gives rise to bands of enhanced transmission in spectra obtained in p-polarized light. The dashed lines outlining these bands in Fig. 2(b) represent the dispersions of surface-plasmon polaritons at the surface of a metal film possessing a hexagonal lattice of scatterers at the Au-opal and Au-air interfaces, respectively,

$$k(\omega) = \pm\sqrt{k_{SPP}(\omega)^2 - \left(\frac{2\pi}{D\sqrt{3}}(2j-i)\right)^2} - \frac{2\pi i}{D}, \quad i,j = 0, \pm 1, \pm 2, \ldots, \tag{2}$$

where $k_{SPP}(\omega) = \frac{2\pi}{\lambda}\sqrt{\frac{\varepsilon_d \varepsilon_m}{\varepsilon_d+\varepsilon_m}}$ and ε_m, ε_d—dielectric constants of the metal and the adjacent dielectric. The adherence of the band of enhanced transmission to dispersions of (11) surface-plasmon-polariton modes at the Au-air and Au-opal interfaces let us assign this effect of plasmon polaritons [22]. The absence of these plasmon bands in the transmission spectra recorded in s-polarized light supports this conclusion.

IV. TAMM STATE

Let us interrogate these spectra for the presence of less obvious changes of the (111) resonance. The (111) transmission dip in the Au opal becomes slightly narrower compared to that in the spectrum of the bare opal due the "blueshift" of the low-frequency edge of transmission dip [curves T^{O} and $T^{\text{Au-O}}$ in Fig. 2(c)]. The bandwidth of the diffraction maximum in the reflectance spectrum of the bare opal is also reduced [curves R^{O} and $R^{\text{Au-O}}$ in Fig. 2(d)]. Moreover, the narrow minimum appears at the band edge at $D/\lambda \approx 0.43$ in registry with the squeezed transmission minimum.

This modification of the Bragg resonance bears similarities and differences with the standard appearance of the Tamm state. To date Tamm states have been investigated using $\lambda/4$ Bragg multilayers possessing the metal film, which interfaces the layer of the dielectric made of the higher refractive index material. Without the metal coating such a multilayer demonstrates the minimum in the transmission spectrum, namely, the photonic stop band if the destructive interference of the wave completing the round trip inside the Bragg mirror takes place. Application of the metal mirror reverses the phase of the wave when it is reflected at the former dielectric-air interface of the Bragg mirror. Consequently, the interference changes to the constructive one due to the 2π-proportional phase difference acquired along the round trip. The respective transmission peak, the Tamm state, appears inside the stop band because the effective refractive index of the multilayer is the mean value of the refractive indices of the dielectric layers.

In contrast, if the Bragg mirror ends up with the layer of the lower refractive index, the interference is always destructive, whether or not there is a metal mirror at the Bragg multilayer surface, and no Tamm state occurs [26]. This is exactly the case of the opal assembled on a flat metal surface because the opal density vanishes towards the contact point of the spheres with the metal.

How to acquire the Tamm state in the latter case? Let us consider the $\frac{1}{4}$-wavelength Bragg multilayer with the refractive index profile across planes adopted to that along the [111] axis of the opal [36] and averaged in lateral directions [Fig. 3(a)]. To finish, this Bragg mirror bears the 50-nm-thick Au coating. It is known that the spectral position of the Tamm state can be changed by truncating the high refractive index layer of the Bragg reflector in contact with the metal [17]. By analogy, we trimmed the topmost low-index layer. This truncation introduces the phase shift to the traveling wave that moves the resonance frequency of the asymmetric resonator towards the photonic stop band. In this case, light becomes

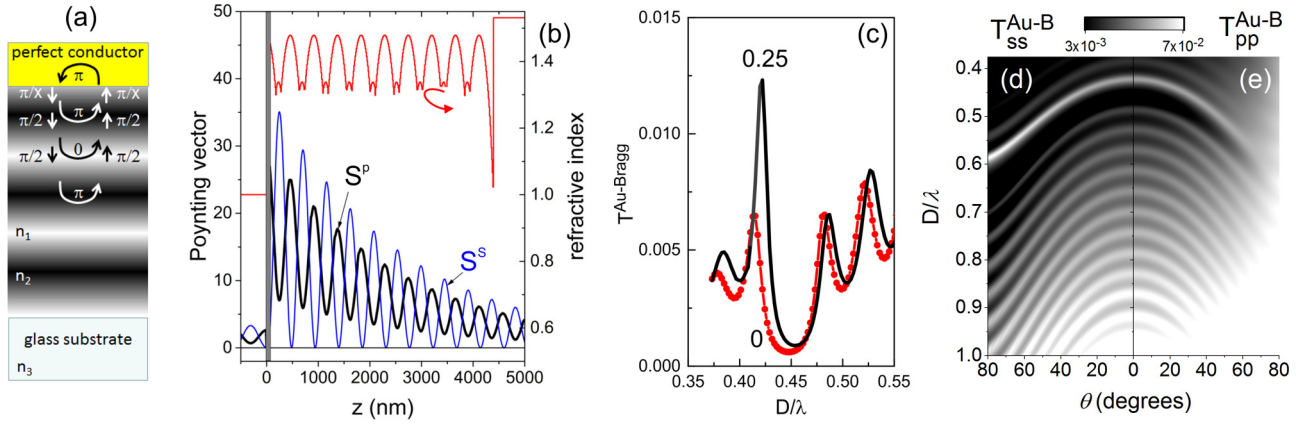

FIG. 3. (a) $\lambda/4$ Bragg multilayer on a glass substrate with the metal layer on top. $n_1 < n_2 < n_3$—refractive indices of layers and a substrate. The arrows, which are labeled with respective phase shifts, indicate the round trip. (b) Decay of the energy flow in the depth of the 50-nm Au-coated Bragg mirror (ten layers). In-plane component Poynting vector normalized on $\sin(\theta)$ is calculated at $\theta = 10^{-5\circ}$ for the s- and p-polarized light, respectively. The refractive index profile is shown at the top, and the gray box corresponds to the metal film. (c) Transmission spectra of a Au-Bragg mirror at 0% and 25% truncations of the low refractive index layer. (d) and (e) Transmission maps of the 25% truncated Au-Bragg mirror in s- and p-polarized light, respectively. The bright band along the low-frequency band edge is the Tamm surface state.

effectively localized at the gold-multilayer interface, such as in the standard Tamm state configuration [Fig. 3(b)]. Modeling shows that the 25% reduction of the thickness of the $\frac{1}{4}$-wavelength-thick low-index layer is sufficient to produce the Tamm state in the stop-band edge [compare Figs. 2 and 3(c)].

Thus, the observed modification of the opal stop band in a Au opal meets the requirements for the Tamm defect state [15]. This observation suggests that the metal coating effectively cuts ~25% of the (111) plane in metal-coated opals in qualitative agreement with the surface profile of the metal coating on the opal surface [Fig. 1(b)].

Note that the width of the (111) Tamm state is about the width of the Fabry-Pérot oscillations in agreement with the interference nature of this effect. The experimentally achieved transmission enhancement at the Tamm state is almost 100 times lower compared to that prescribed by simulations for the ten-period strong Bragg reflector. Provisionally, this is the cumulative effect of neglecting the lateral profile of (111) opal planes, the pointlike connectivity of metal semishells, the intrinsic opal disorder, and the angle diversion of the incident light beam.

V. SURFACE STATES AT HIGH FREQUENCIES

The next spectral feature of the transmission spectrum above the (111) band is the extraordinary transmission peak occurring at a frequency of $D/\lambda \approx 0.77$ due to tunneling of surface-plasmon polaritons located at the Au-opal interface [22,37] [Fig. 4(a)]. Furthermore, at $D/\lambda > 0.8$ one can find a broad transmission minimum that corresponds to the superimposed (222), (220), and (200) diffraction resonances. Yet another weak peak of the extraordinary transmission related to surface plasmons residing at the Au-air interface is observed above this transmission minimum at $D/\lambda \approx 0.92$. We will show that these plasmon-polariton surface states coexist with the Tamm surface states.

In order to emphasize changes associated with the additional metal film we plotted the relative transmission spectrum—the ratio of transmission spectra of hybrid and bare opals $T^{\text{Au-O}}/T^{\text{O}}$[Fig. 4(b)]. First, the low magnitude of the relative transmission spectra appreciates the light attenuation by the metal film. In particular, the Au film reduces the transmission of the Au opal by 27 times to that of the bare opal, respectively [Fig. 4(a)]. Second, this plot demonstrates a twofold relative transmission enhancement at the low-frequency edge of the (111) stop band that is the signature of the Tamm state. Third, the relative transmission spectrum reveals pronounced peaks all over the spectrum. For example, four times transmission enhancement is associated with the extraordinary transmission peak and up to five times enhancement—with the above-mentioned superimposed diffraction resonances. Partly, the high magnitude of the high-frequency bands in the relative transmission spectrum can be explained by the progressively increasing transparency of the gold film towards the peak of interband transitions at ~500 nm [34].

For the sake of generality, in Figs. 4(c) and 4(d) we show the spectra of the silver-coated opal assembled from 430-nm spheres and coated with a 30-nm-thick Ag film. This comparison illustrates the common character of the surface states occurring in the metal-coated opals. Quantitatively, the relative transmission of the Ag opal is almost five times higher compared to that in the Au opal. On one hand, the difference can be explained taking into account the lower light absorption/higher transmission of the Ag film, moreover, no absorptive interband electron transitions take place in a silver film in the considered spectral range. This observation agrees with the inhibiting role of light losses on a metal mirror. On the other hand, the opal film in the Au opal is thinner compared to the film of the Ag opal [20 vs 27 (111) planes] leading to weaker Bragg reflectivity of the former [compare magnitudes of (111) resonances in Figs. 4(a) and 4(c)]. This observation points to the need in the highly

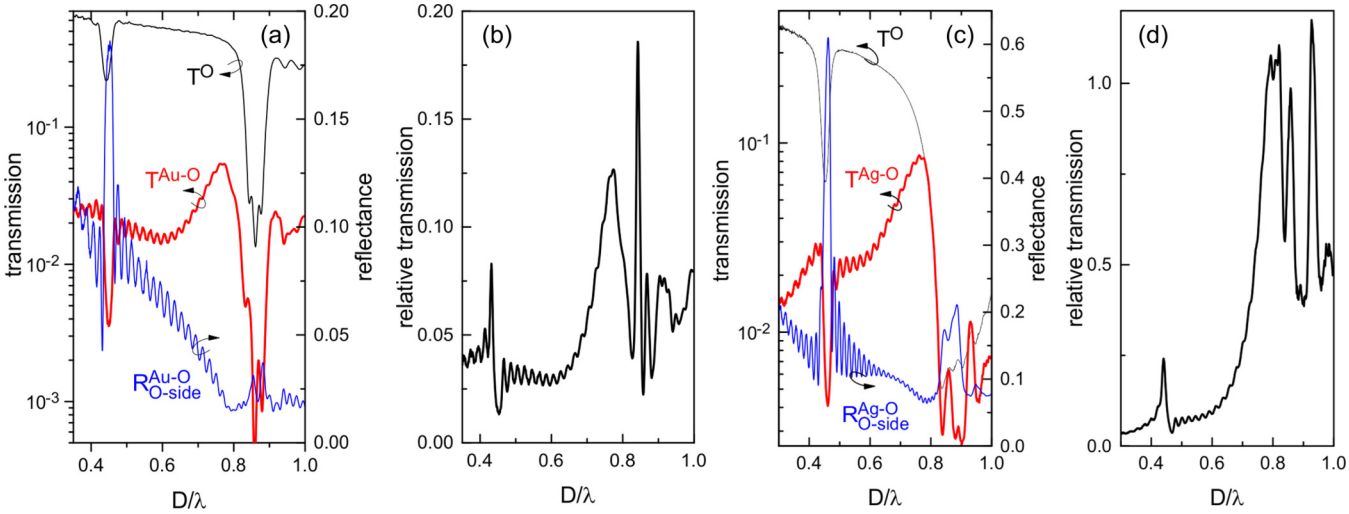

FIG. 4. (a) Transmission spectra of 50-nm Au-coated ($T^{\text{Au-O}}$, thick line) and bare (T^{O}, thin line) opals assembled from 560 nm and in comparison with the reflectance spectrum of a Au opal obtained through the glass substrate by illuminating the opal side of the Au-opal hybrid sample ($R^{\text{Au-O}}_{\text{Oside}}$), respectively. (c) The same for the 30-nm Ag-coated opal assembled from 430-nm spheres. (b) and (d) Relative transmission spectra of Au-O and Ag-O samples.

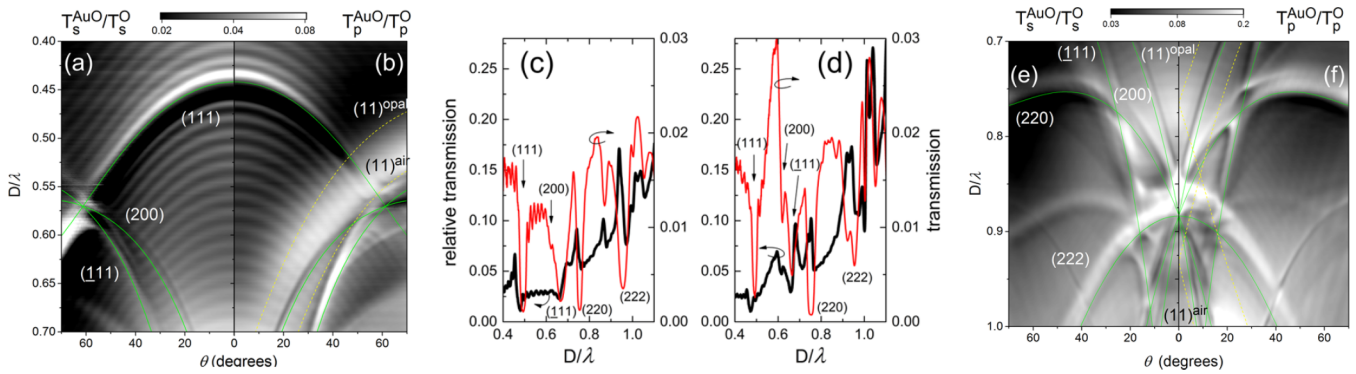

FIG. 5. (a), (b), (e), and (f) Maps of the relative transmission of 50-nm Au-opal samples assembled from 560-nm spheres at low- and high-frequency spectral intervals. Diffraction and surface-plasmon-polariton resonances are the same as in Figs. 2(a) and 2(b). (c) and (d) Comparison of relative transmission spectra (thick lines) at $\theta = 35^\circ$ with respective transmission spectra (thin lines) in s-polarized [panel (c)] and p-polarized [panel (d)] light.

reflective Bragg mirror for obtaining more pronounced Tamm states.

VI. TAMM STATES AT OBLIQUE LIGHT INCIDENCE

Tamm states plotted as a function of the incident angle form a continuous band. The angle dispersion of this Tamm band in the calculated transmission spectra of the truncated Au-coated Bragg mirror follows rigorously the dispersion of the stop band [Figs. 3(d) and 3(e)]. Moreover, the polarization anisotropy of the Tamm band uniquely agrees with the anisotropy of the stop band. Indeed, the Tamm band in relative transmission maps of the Au opal obeys the same behavior for both polarizations of the incident light as long as it does not interfere with the other resonances of the hybrid structure [Figs. 5(a) and 5(b)].

An opal photonic crystal possesses the second order of the (111) resonance, the (222) resonance, which follows the same dispersion [21]. Since the high-frequency resonances are stronger affected by scattering at lattice inhomogeneities, the light attenuation in the (222) minimum is weaker compared to that in the (111) one [Figs. 2(a) and 2(b)]. Respectively, for the same reason the (222) Tamm state in the relative transmission spectrum is weak and stretches across almost the whole transmission minimum bandwidth [compare (111) and (222) Tamm states in Fig. 5].

Other diffraction resonances of the three-dimensional opal lattice can be associated with the collection of the high Miller index crystal planes acting as Bragg reflectors, which are not coplanar to the opal film surface and, hence, to the plane of the metal film. Due to the threefold rotation symmetry of the fcc lattice, the respective diffraction orders will not be able to complete the round trip being specularly reflected at the metal coating, except for the ΓW directions in the opal Brillouin zone [Fig. 1(c)] where the (200) and $(\bar{1}11)$ diffraction orders are collinear to the (111) order. In Fig. 5(a) one can see the respective Tamm state peculiarities at the crossing of the (111), (200), and $(\bar{1}11)$ dispersions in the vicinity of $\theta \approx 60^\circ$.

Surprisingly, the relative transmission spectra of the Au opal plotted against their transmission spectra show the peaks at the edges of the transmission minima in a similar manner to the (111) Tamm state [Figs. 5(c) and 5(d)]. In order to avoid the erroneous comparison, we calculated the relative transmission spectra by selecting bare and metal-coated opal films of the same number of (111) planes as well as repeated this procedure for opals with different coating thicknesses and different sphere sizes. Since the observed modifications of diffraction minima are qualitatively the same in all studied samples, we assumed the general character of the observed effect.

The resonance states associated with diffraction resonances at high Miller index planes appear differently for respective Bragg mirrors. The (200) and $(\bar{1}11)$ resonances are only marginally affected by the metal coating in spectra of s-polarized light [Fig. 5(c)]. Oppositely, in p-polarized light they appear more vulnerable [Fig. 5(d)]. Provisionally, the reason for this difference is their spectral overlap with diffractively coupled surface-plasmon polaritons [Fig. 5(b)]. Whether or not Tamm resonances and surface-plasmon polaritons interact with each other is the matter of a separate investigation.

The (220) resonance possesses the Tamm state that is attached to the edge of the respective diffraction minimum [Figs. 4(e) and 4(f)], i.e., it obeys the same scenario as the (111) resonance. Noteworthy, this Tamm state is more pronounced compared to the defect states of other diffraction orders. It is instructive to note that the angle between (111) and (220) planes is about 35.3°, i.e., it is smaller compared to angles with (200) and $(\bar{1}11)$ planes, which are 54.7° and 70.5°, respectively. This observation lets us assume the link between the magnitude of the Tamm state and the declination of the diffraction orders from the (111) order.

The modification of opal diffraction resonances that is observed in a Au opal at the so-called avoided band crossing further supports its assignment of the Tamm state. This anticrossing is the multiple wave diffraction phenomenon occurring in three-dimensional photonic crystals when the dispersions of diffraction resonances originating from different crystal planes become interrupted instead of crossing each other [38]. As the result, no collinearly propagating diffraction orders of the same frequency and, correspondingly, no superimposed Bragg mirrors exist in the lattice along the crossing direction. We consider the anticrossing of $(\bar{1}11)$ and (220) resonances taking place at $D/\lambda = 0.787$ and centered at an external angle of light incidence of $\theta = 22^\circ$ where the related transmission dips in Au-opal spectra become shallow [Fig. 6(a)]. This angle corresponds to the internal angle of incidence of 17.4° since the angle between these

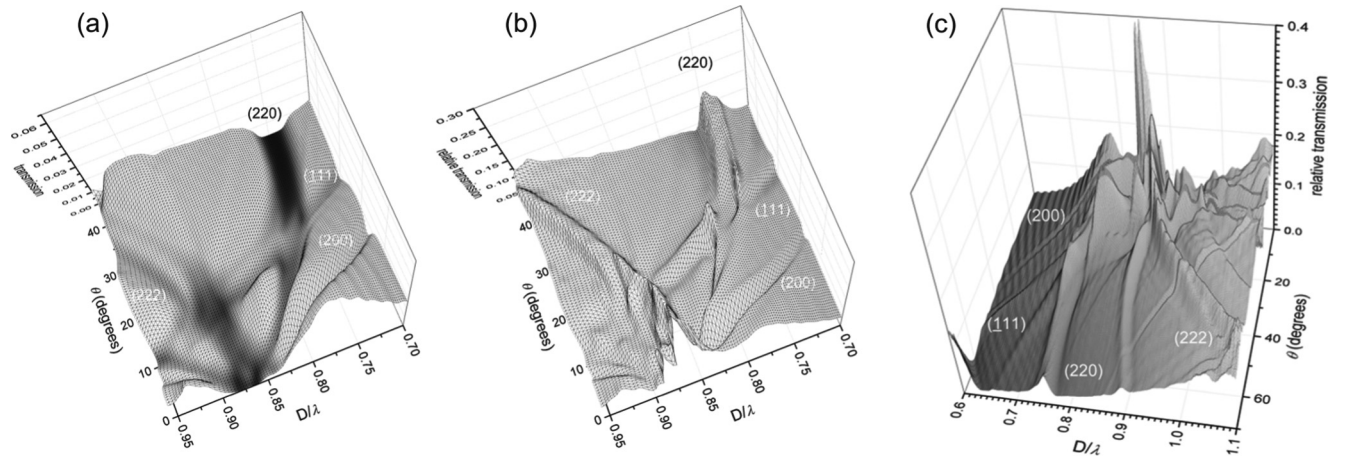

FIG. 6. (a) and (b) Avoided band crossings in transmission and relative transmission spectra of the Au-opal sample in p-polarized light, respectively. (c) Tamm bands associated with high Miller index planes and the extraordinary transmission peak of surface-plasmon polaritons in relative transmission spectra of the Au-opal sample in s-polarized light.

planes is 34.8°. The respective bands of relatively enhanced transmission follow the edges of both transmission minima and disappear as soon as the Bragg reflection vanishes at the anticrossing [Fig. 6(b)]. Notably, almost doubling of the transmission enhancement takes place at the beginning of the avoided band crossing region where the multiple wave diffraction becomes substantial [Fig. 6(b)].

Overall, relative transmission spectra demonstrate rims decorating diffraction resonances of high-index planes [Fig. 6(c)]. The strongest changes are observed close to the normal light incidence. Remarkably, the peak of the relative transmission centered at $D/\lambda \approx 0.86$ and corresponding to overlapping (222), (200), and (220) resonances rises twice as high as the extraordinary transmission peak at $D/\lambda \approx 0.78$, which is caused by diffractively excited true surface waves—surface-plasmon polaritons.

In order to give an idea about the magnitude of the transmission modification induced by the application of deeply corrugated and perforated metal film on the opal surface, we show in Fig. 7 the transmission spectra obtained after rectification with respect to the transmission of the flat metal film and the light diffraction/scattering in the volume of an opal photonic crystal $T_p^{\text{Au-O}}/T_p^{\text{O}}/T_p^{\text{Au}}$. Clearly, surface waves, namely, plasmon polaritons and Tamm defect states, are associated with the relative transmission enhancement. This procedure brings forward the (111) Tamm state as the most pronounced effect. Other Tamm states are also uniquely attached to diffraction resonances.

This observation suggests that the transparency of semishells not only exceeds by almost ten times the transparency of the flat metal film of the same nominal thickness, but its dielectric function also follows the different dispersion due to enhanced absorption in the spectral range of plasmonic excitations [39].

VII. ORIGIN OF UNCONVENTIONAL TAMM STATES IN METAL-COATED OPALS

How can we prove that weakening of diffraction resonances in the Au opal is the signature of surface states? Since Bragg reflectors related to high Miller index planes are not parallel to the metal coating, the planar resonator model fails in this case. Let us consider light scattering at metal semishells. If the period and depth of the metal corrugation become comparable to the operating wavelength, the electromagnetic field can be confined in corrugations. Modeling shows that a semishell should possess its own localized cavity plasmon resonances, moreover, they survive if several semishells are joined together [28]. According to our calculations, if $D/n\lambda \leqslant 1$, where n is the refractive index of the dielectric sphere,

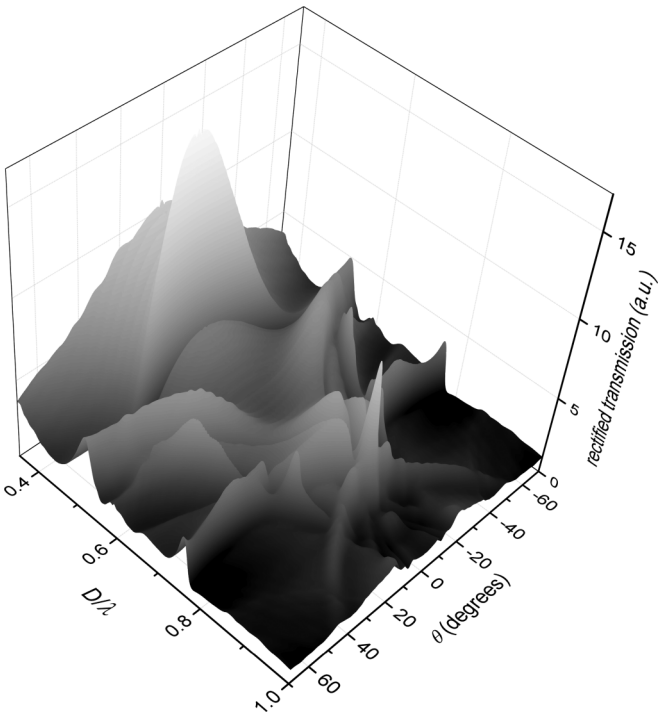

FIG. 7. Surface states in the spectra of the rectified transmission of the Au-opal hybrid $T_p^{\text{Au-O}}/T_p^{\text{O}}/T_p^{\text{Au}}$, obtained in p-polarized light. Transmission minima correspond to diffraction resonances. Transmission bands—correspond to surface states.

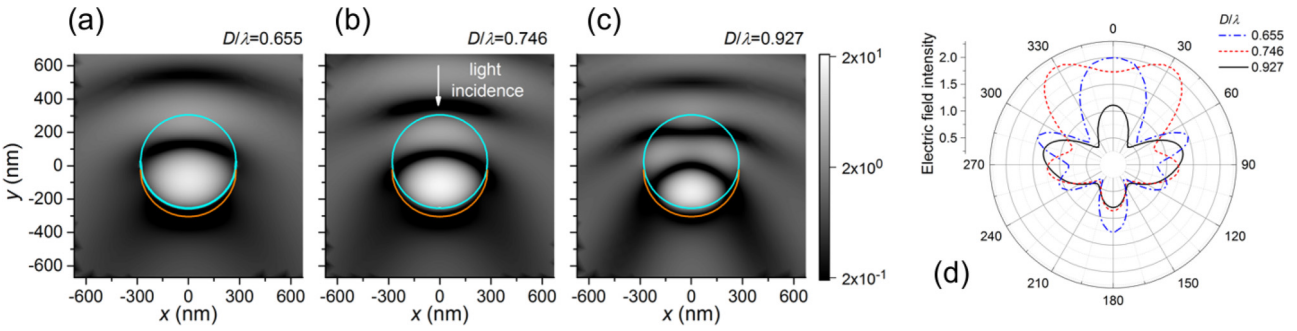

FIG. 8. Light scattering at metal semishells. (a)–(c) Calculated cross sections of the electric-field intensity of light scattered by a gold semishell (50-nm Au coating on a 560-nm PMMA sphere) at different reduced frequencies (frequencies label the panels). The PMMA sphere and semishell are indicated by the circle and the crescent, respectively. (d) Angle diagrams of the scattered light intensities calculated at the fixed distance 650 nm from the center of PMMA sphere for different reduced frequencies.

the localized resonances of the semishells are not sharp and overlap in the considered spectral range [Figs. 8(a)–8(c)]. Therefore, the field becomes confined at the metal-dielectric interface as soon as light approaches the semishells. Since light in the volume of the opal photonic crystal is transported by diffraction orders, the localized resonances appear in registry with these resonances.

The semishell cavity resonance looks similar to the field confinement in the asymmetric Fabry-Pérot resonator at the interface between the metal coating and the Bragg mirror. Remarkably, the maximum of the field intensity is located inside the metal semishell at a certain distance from its geometrical circumference (Fig. 8). This configuration is analogous to the truncation of the low-index outer layer of the opal reflector, which is the necessary condition for placing the Tamm state in the photonic stop band as was derived from the flat resonator model (Fig. 3).

The localized resonance of a metal semishell is capable of the light scattering with the broad angular diagram. Consequently, the light scattering at the semishell is dramatically different from the specular reflection of light by a flat mirror. The moderate changing in the scattering diagram along the frequency change [Fig. 8(d)] is consistent with the weak resonance character of the local semishell resonance. In our opinion, this resonance is able to maintain the substantial flow of backscattered light intensity, which can constructively interfere with the incident diffraction orders over the broad range of incidence angles. The latter is a qualifying property of the Tamm surface state that is embedded in the photonic stop band.

Thus, scattering of diffraction orders at metal semishells of a Au-opal functionally replaces the specular reflection at the metal mirror of the Bragg multilayer. Quantitatively, the weakness of such a resonance in transmission/reflectance spectra follows the low efficiency of the backscattering of the corrugated metal mirror compared to the reflectivity of the flat metal mirror. This consideration can be illustrated by comparing the strength of the (111) Tamm state in the Au opal and in the Bragg mirror model [Figs. 3(d) and 3(e) and 5(a) and 5(b)].

Supposing the Tamm surface states exist for misaligned Bragg and metal reflectors, how broad should the scattering diagram of the semishell be to maintain them in the opal? For example, if the external incident angle varies from 0° to 80° with respect to the [111] axis by scanning the incident angle in the $L\Gamma W$ cross section of the Brillouin zone [Fig. 1(c)], the internal incidence angle spans between 17° and 35° with respect to the [220] axis, between 24° and 54° for [200] axis, and between 35° and 70° for the [11$\bar{1}$] axis. Apparently, the relatively small deviation of the (220) diffraction order is the reason for the higher visibility of the respective Tamm state compared to other resonances and its persistence over the broad range of incident angles.

Another peculiarity of diffraction at high Miller index planes of three-dimensional photonic crystals is their rapid change with the azimuth rotation of the plane of light incidence for a fixed angle of incidence. For the same angle of incidence with respect to the (111) plane, the alignment of the plane of incidence with the $L\Gamma K$ cross section of the Brillouin zone of the opal lattice shifts the quoted angle ranges to 0°–35°, 45°–54°, and 25°–70°, respectively for the (220), (200), and (11$\bar{1}$) planes [21]. Hence, the azimuth rotation of the opal lattice transfers in the patchy appearance of respective Tamm states according to the threefold rotation axis symmetry of the fcc lattice in contrast to the azimuth-independent (111) Tamm state.

Further consideration of the Au-opal optical response should take into account the light confinement in between touching semishells. These are the nonresonant surface states of plasmonic nature, which are responsible for the broadband light absorption in the grooves of profiled metal film [39,40]. The respective light scattering also takes place at the opal-metal interface, but the evaluation of this contribution will be addressed in following studies.

VIII. SUMMARY

Summarizing, using the heterostructuring approach to engineer the photonic materials we investigated the effect of metal coatings on diffraction resonances of three-dimensional photonic crystals. We prepared metal film-terminated opal photonic crystals and observed optical resonances, which appear in registry with diffraction resonances. Whereas the deposition of metal films on photonic crystals does not affect the diffraction in crystal volumes, metal coating induces the constructive interference of diffracted and backreflected

light in the narrow spectral interval within the diffraction resonance bandwidth. This resonance reveals itself as the band of high transmission/low reflectance at the edge of the respective transmission minimum/reflectance maximum of a metal-terminated opal.

The constructive interference leads to the light confinement at the metal-photonic crystal interface. Such resonances can be referred to as defect states because they are associated with the interruption of the lattice periodicity. In contrast to the conventional optical Tamm state, which occurs due to electromagnetic field confinement in the flat asymmetric Fabry-Pérot resonator between metal and Bragg mirrors, the unconventional Tamm states can be referred to as the field localization in metal semishells. The mechanism behind the Tamm states in a metal-terminated opal is the constructive interference of incident and backscattered diffraction orders.

The angular-broad scattering diagram of the semishells supports the resonance conditions for diffraction orders approaching the interface at arbitrary angles but at the cost of the low reflectivity. All but (111) resonances in the metal-coated opals are concealed in diffraction resonances. Functionally, the Tamm surface states of three-dimensional photonic crystals reduce the bandwidth and the strength of diffraction resonances as compared to these parameters in bare photonic crystals. Oppositely, purposive positioning and optimization of surface resonance states can be exploited to build up efficient light sources, absorbers, sensors, and nonlinear transducers. In our opinion, keeping the integrated photonic circuits in mind, designing surface states is of competing significance compared to other methods of controlling the optical properties of photonic crystals.

ACKNOWLEDGMENTS

The work of S.G.R. was partly supported by the Deutsche Forschungsgemeinschaft Cluster of Excellence "Engineering of Advanced Materials" of FAU of Erlangen (Germany) and the EU IRSES project Phantasy. The authors are grateful to R. Klupp-Taylor for taking the SEM image.

[1] J. D. Joannopoulos, S. G. Johnson, J. N. Winn, and R. D. Meade, *Photonic Crystals: Molding the Flow of Light*, 2nd ed. (Princeton University Press, Princeton, 2008).
[2] I. Tamm, Phys. Z. Sowjetunion **1**, 733 (1932).
[3] H. Ohno, E. E. Mendez, J. A. Brum, J. M. Hong, F. Agulló-Rueda, L. L. Chang, and L. Esaki, Phys. Rev. Lett. **64**, 2555 (1990).
[4] E. Istrate and E. H. Sargent, Rev. Mod. Phys. **78**, 455 (2006).
[5] S. G. Romanov, N. Gaponik, A. Eychmüller, A. L. Rogach, V. G. Solovyev, D. N. Chigrin and C. M. Sotomayor Torres, *in Photonic Crystals*, edited by K. Busch, S. Lölkes, R. Wehrspohn, and H. Föll (Wiley-VCH, Weinheim, 2004), pp. 132–152.
[6] L. D. Landau, E. M. Lifshitz, and L. P. Pitaevskii, *Electrodynamics of Continuous Media*, 2nd ed. (Butterworth Heinemann, Oxford, 1995).
[7] P. Yeh, A. Yariv, and A. Y. Cho, Appl. Phys. Lett. **32**, 104 (1978).
[8] R. D. Meade, K. D. Brommer, A. M. Rappe, and J. D. Joannopoulos, Phys. Rev. B **44**, 10961 (1991).
[9] W. M. Robertson, G. Arjavalingam, R. D. Meade, K. D. Brommer, A. M. Rappe, and J. D. Joannopoulos, Opt. Lett. **18**, 528 (1993).
[10] S. Enoch, E. Popov, and N. Bonod, Phys. Rev. B **72**, 155101 (2005).
[11] C. Tserkezis, N. Stefanou, G. Gantzounis, and N. Papanikolaou, Phys. Rev. B **84**, 115455 (2011).
[12] B. Wang, W. Dai, A. Fang, L. Zhang, G. Tuttle, T. Koschny, and C. M. Soukoulis, Phys. Rev. B **74**, 195104 (2006).
[13] K. Ishizaki and S. Noda, Nature(London) **460**, 367 (2009).
[14] T. Goto, A. V. Dorofeenko, A. M. Merzlikin, A. V. Baryshev, A. P. Vinogradov, M. Inoue, A. A. Lisyansky, and A. B. Granovsky, Phys. Rev. Lett. **101**, 113902 (2008).
[15] A. P. Vinogradov, A. V. Dorofeenko, S. G. Erokhin, M. Inoue, A. A. Lisyansky, A. M. Merzlikin, and A. B. Granovsky, Phys. Rev. B **74**, 045128 (2006).
[16] A. P. Vinogradov, A.V. Dorofeenko, A. M. Merzlikin, and A. A. Lisyansky, Phys.-Usp. **53**, 243 (2010).
[17] M. Kaliteevski, I. Iorsh, S. Brand, R. A. Abram, J. M. Chamberlain, A. V. Kavokin, and I. A. Shelykh, Phys. Rev. B **76**, 165415 (2007).
[18] G. Lheureux, C. Symonds, S. Azzini, J. Bellessa, J.-P. Hugonin, J.-J. Greffet, A. Lemaître, P. Senellart, SPIE Newsroom, doi:10.1117/2.1201310.005085.
[19] Y. Gong, X. Liu, H. Lu, L. Wang, and G. Wang, Opt. Express **19**, 18393 (2011).
[20] J. F. Galisteo-López, M. Ibisate, R. Sapienza, L. S. Froufe-Pérez, Á. Blanco, and C. López, Adv. Mater. **23**, 30 (2011).
[21] J. Küchenmeister, C. Wolff, K. Busch, U. Peschel, and S. G. Romanov, Adv. Opt. Mater. **1**, 952 (2013).
[22] S. A. Maier, *Plasmonics: Fundamentals and Applications* (Springer, New York, 2007).
[23] B. Ding, M. E. Pemble, A. V. Korovin, U. Peschel, and S. G. Romanov, Phys. Rev. B **82**, 035119 (2010).
[24] S. G. Romanov, A. Regensburger, A. V. Korovin, and U. Peschel, Adv. Mater. **23**, 2515 (2011).
[25] S. G. Romanov, S. Orlov, A. V. Korovin, G. P. Chuiko, A. Regensburger, A. S. Romanova, A. Kriesch, and U. Peschel, Phys. Rev. B **86**, 195145 (2012).
[26] S. G. Romanov, A. Regensburger, A. V. Korovin, A. S. Romanova, and U. Peschel, Phys. Rev. B **88**, 125418 (2013).
[27] M. E. Sasin, R. P. Seisyan, M. A. Kaliteevskii, S. Brand, R. A. Abram, J. M. Chamberlain, I. V. Iorsh, I. A. Shelykh, A. Y. Egorov, A. P. Vasil'ev, V. S. Mikhrin, and A. V. Kavokin, Superlattices Microstruct. **47**, 44 (2010).
[28] A. I. Maaroof, M. B. Cortie, N. Harris, and L. Wieczorek, Small **4**, 2292 (2008).
[29] M. Müller, R. Zentel, T. Maka, S. G. Romanov, and C. M. Sotomayor Torres, Chem. Mater. **12**, 2508 (2000).
[30] W. Khunsin, A. Amann, G. Kocher, S. G. Romanov, S. Pullteap, H. C. Seat, E. P. O'Reilly, R. Zentel, and C. M. Sotomayor Torres, Adv. Funct. Mater. **22**, 1812 (2012).

[31] L. Landstrom, D. Brodoceanu, D. Bauerle, F. J. Garcia-Vidal, S. G. Rodrigo, and L. Martin-Moreno, Opt. Express **17**, 761 (2009).
[32] A. Taflove, *Computational Electrodynamics: The Finite-Difference Time-Domain Method* (Artech House, Boston, 2005).
[33] www.lumerical.com.
[34] P. B. Johnson and R. W. Christy, Phys. Rev. B **6**, 4370 (1972).
[35] W. Khunsin, G. Kocher, S. G. Romanov, and C. M. Sotomayor Torres, Adv. Funct. Mater. **18**, 2471 (2008).
[36] G. M. Gajiev, V. G. Golubev, D. A. Kurdyukov, A. V. Medvedev, A. B. Pevtsov, A. V. Sel'kin, and V. V. Travnikov, Phys. Rev. B **72**, 205115(2005).
[37] T. W. Ebbesen, H. J. Lezec, H. F. Ghaemi, T. Thio, and P. A. Wolff, Nature (London) **391**, 667 (1998).
[38] S. G. Romanov, T. Maka, C. M. Sotomayor Torres, M. Müller, R. Zentel, D. Cassagne, J. Manzanares-Martinez, and C. Jouanin, Phys. Rev. E **63**, 056603 (2001).
[39] B. Ding, M. Bardosova, M. E. Pemble, A. V. Korovin, U. Peschel, and S. G. Romanov, Adv. Funct. Mater. **21**, 4182 (2011)
[40] T. Søndergaard, S. M. Novikov, T. Holmgaard, R. L. Eriksen, J. Beermann, Z. Han, K. Pedersen, and S. I. Bozhevolnyi, Nat. Commun. **3**, 969 (2012).